
Mind the (optimality) Gap: A Gap-Aware Learning Rate Scheduler for Adversarial Nets

Hussein Hazimeh
Google Research

Natalia Ponomareva
Google Research

Abstract

Adversarial nets have proved to be powerful in various domains including generative modeling (GANs), transfer learning, and fairness. However, successfully training adversarial nets using first-order methods remains a major challenge. Typically, careful choices of the learning rates are needed to maintain the delicate balance between the competing networks. In this paper, we design a novel learning rate scheduler that dynamically adapts the learning rate of the adversary to maintain the right balance. The scheduler is driven by the fact that *the loss of an ideal adversarial net is a constant known a priori*. The scheduler is thus designed to keep the loss of the optimized adversarial net close to that of an ideal network. We run large-scale experiments to study the effectiveness of the scheduler on two popular applications: GANs for image generation and adversarial nets for domain adaptation. Our experiments indicate that adversarial nets trained with the scheduler are less likely to diverge and require significantly less tuning. For example, on CelebA, a GAN with the scheduler requires only one-tenth of the tuning budget needed without a scheduler. Moreover, the scheduler leads to statistically significant improvements in model quality, reaching up to 27% in Frechet Inception Distance for image generation and 3% in test accuracy for domain adaptation.

Adversarial Nets (GANs) are a foundational example of this class of models (Goodfellow et al., 2014). Given a finite sample from a target distribution, a GAN aims to generate more samples from that distribution. This is achieved by training two competing networks. A generator G transforms noise samples into the sample space of the target distribution, and a discriminator D attempts to distinguish between the real and generated samples. To generate realistic samples, G is trained to fool D . Adversarial nets used in domains other than generative modeling follow the same principle of training two competing networks.

Training an adversarial net typically requires solving a non-convex, non-concave min-max optimization problem, which is notoriously challenging (Razaviyayn et al., 2020). In practice, first-order methods are commonly used as a heuristic for this problem. One popular choice is Stochastic Gradient Descent Ascent (SGDA), which is an extension of SGD that takes gradient descent and ascent steps over the min and max problems, respectively¹. SGDA and its adaptive variants (e.g., based on Adam) are the defacto standard for optimizing adversarial nets (Ganin et al., 2016; Radford et al., 2016; Arjovsky et al., 2017). These methods require choosing two base learning rates²; one for each competing network. However, adversarial nets are very sensitive to the learning rates (Lucic et al., 2018), and careful choices are needed to maintain a balance between the competing networks. In practice, the same learning rate is often used for both networks (Wang et al., 2021), even though decoupled rates can lead to improvements (Heusel et al., 2017). The base learning rates typically used in the literature are constant, but could also be decayed during training. In either case, these rates do not depend on the current state of the network.

In this paper, we argue that a *dynamic* choice of the base learning rate that responds to the current state of the adversarial net can significantly enhance training. Specifically, we propose a learning rate scheduler that dynamically changes the base learning rate of existing optimizers (e.g., Adam), based on the current loss of the network. Our scheduler is

1 Introduction

Adversarial networks have proved successful in generative modeling (Goodfellow et al., 2014), domain adaptation (Ganin et al., 2016), fairness (Zhang et al., 2018), privacy (Abadi and Andersen, 2016), and other domains. Generative

Proceedings of the 26th International Conference on Artificial Intelligence and Statistics (AISTATS) 2023, TBD, USA. PMLR: Volume XXX. Copyright 2023 by the author(s).

¹The steps could be simultaneous or alternating.

²We use the term base learning rate to refer to the base learning rate in adaptive optimizers and to the learning rate of SGDA.

driven by the following key observation: in many popular formulations, *the loss of an ideal adversarial net is a constant known a priori*. For example, an ideal GAN is one in which the distributions of the real and generated samples match. Therefore, we can define an *optimality gap*, which refers to the gap (absolute difference) between the losses of the current and ideal adversarial nets.

Our main hypothesis is that adversarial nets with smaller optimality gaps tend to perform better—we present empirical evidence that verifies this hypothesis on different loss functions and datasets. Motivated by this hypothesis, our proposed scheduler keeps track of the optimality gap. At each optimization step, the scheduler decides whether to increase or decrease the base learning rate of the adversary (e.g., discriminator), in order to keep the optimality gap relatively small. The base learning rate of the competing network (e.g., generator) is kept constant, since controlling the loss of the adversary (through its base rate) effectively modifies that of the competing network³.

We demonstrate the effectiveness of the scheduler empirically in two popular use cases: GANs for image generation and Domain Adversarial Neural Nets (DANN) (Ganin et al., 2016) for domain adaptation. We observe that the scheduler significantly reduces the need for tuning (by $\sim 10x$ in many cases) and can lead to statistically significant improvements in the main performance metrics (image quality or accuracy) on five benchmark datasets.

Contributions: (i) We present statistical evidence showing that GANs with smaller optimality gaps tend to generate higher quality samples (see Sec. 2). (ii) Motivated by the latter evidence, we propose a novel scheduler that adapts the base learning rate of the adversary to keep the optimality gap relatively small and maintain a balance with the competing network (see Sec. 3). (iii) We carry out a large-scale statistical study on GANs and DANN to compare the performance of the scheduler with popular alternatives. Specifically, we study how the tuning budget and weight initialization affect performance by systematically training over 25,000 GANs. The results indicate that the scheduler can reduce the need for tuning by $\sim 10x$, improve Frechet Inception Distance in GANs by up to 27%, and improve accuracy in DANN by up to 3% (see Sec. 4). We provide a simple open-source implementation⁴ of the scheduler that can be used with any existing optimizer.

1.1 Related Work

Gradient-based methods for non-convex, non-concave min-max problems are known to face difficulties during training

³If the game is zero-sum, an increase in the objective of the adversary will lead to a decrease in the objective of the competing network with an equal magnitude (and vice versa).

⁴https://github.com/google-research/google-research/tree/master/adversarial_nets_lr_scheduler

and may generally fail to achieve even simple notions of stationarity (Razaviyayn et al., 2020). In the context of GANs, there has been active research on stabilizing training (with different notions of stability). One important line of work introduces new loss functions or formulations that may be more amenable to first-order methods (e.g., via additional smoothness or avoiding vanishing gradients) (Li et al., 2015; Arjovsky et al., 2017; Mao et al., 2017; Zhao et al., 2017; Nowozin et al., 2016; Gulrajani et al., 2017). Another related approach is to augment existing GAN loss functions with regularizers or perform simple modifications to SGDA (which may be interpreted as regularization) to improve stability (Che et al., 2017; Mescheder et al., 2017; Nagarajan and Kolter, 2017; Yadav et al., 2018; Mescheder et al., 2018; Xu et al., 2020). Improved architectures have also been vital in successfully training GANs, e.g., see Radford et al. (2016); Neyshabur et al. (2017); Lee et al. (2021) and the references therein. See also Karras et al. (2020) for improving stability using data augmentation. Fundamental to all the approaches described above is the choice of the (base) learning rates, which effectively controls the balance between the competing networks. The base rates used in the literature are typically fixed, but may also be decayed during training. In either setting, the base rates used do not take into account the current state of the network. The main novelty of our scheduler is that it uses the current state of the network (gauged by the optimality gap) when modifying the learning rate.

2 Adversarial Nets and their Ideal Loss

We start this section by briefly reviewing a few popular variants of GANs and discussing how their ideal loss can be determined a priori. Then, in Section 2.1.1, we discuss how the quality of generated samples correlates with the optimality gap. Finally, in Section 2.2, we introduce DANN and discuss how to estimate its ideal loss.

2.1 Generative Adversarial Nets (GANs)

First, we introduce some notation. Let \mathbb{P}_r be the real distribution and \mathbb{P}_n be some noise distribution. The generator G is a function that maps samples from \mathbb{P}_n to the sample space of \mathbb{P}_r (e.g., space of images). We define \mathbb{P}_g as the distribution of $\tilde{x} := G(z)$ where $z \sim \mathbb{P}_n$, i.e., \mathbb{P}_g is distribution of generated samples. The discriminator D is a function that maps samples from G to a real value.

Standard GAN and its Ideal Loss. The standard GAN introduced by Goodfellow et al. (2014) can be written as:

$$\min_G \max_D \mathbb{E}_{x \sim \mathbb{P}_r} \log D(x) + \mathbb{E}_{\tilde{x} \sim \mathbb{P}_g} \log (1 - D(\tilde{x})),$$

where D in this case outputs a probability. In practice, we have a finite sample from \mathbb{P}_r so it is replaced by the corresponding empirical distribution. Moreover, the expectation over \mathbb{P}_g is estimated by sampling from the noise distribution.

We say that a GAN is *ideal* if the generated and real samples follow the same distribution, i.e., $\mathbb{P}_g = \mathbb{P}_r$. When the standard GAN is ideal, the objective function becomes:

$$\max_D \mathbb{E}_{x \sim \mathbb{P}_r} \left[\log D(x) + \log (1 - D(x)) \right].$$

The solution to the problem above is given by $D(x) = 0.5$ for all x in the support of \mathbb{P}_r . Thus, the optimal objective is $-\log(4)$. Throughout the paper, we will be focusing on the loss, i.e., the negative of the utility discussed above. We will denote the optimal loss of D in an ideal GAN by V^* , so in this case $V^* = \log(4)$. This quantity allows for computing the optimality gap, which is essential for the operation of the scheduler.

Popular GAN Variants. While the standard GAN is conceptually appealing, the gradients of the generator may vanish early on during training. To mitigate this issue, Goodfellow et al. (2014) proposed the non-saturating GAN (NSGAN), which uses the same objective for D , but replaces the objective of G with another that (directly) maximizes the probability of the generated samples being real—see Table 1. Similar to the standard GAN, the optimal discriminator loss of an ideal NSGAN is $V^* = \log(4)$.

Many follow-up works have proposed alternative loss functions and divergence measures in attempt to improve the quality of the generated samples, e.g., see Arjovsky et al. (2017); Mao et al. (2017); Nowozin et al. (2016); Li et al. (2017) and Wang et al. (2021) for a survey. In Table 1, we present the objective functions of two popular GAN formulations: Wasserstein GAN (WGAN) and least-squares GAN (LSGAN) (Arjovsky et al., 2017; Mao et al., 2017). WGAN uses a similar formulation to the standard GAN but drops the log, and D outputs a logit (not a probability). Arjovsky et al. (2017) shows that under an optimal k -Lipschitz discriminator, WGAN minimizes the Wasserstein distance between the real and generated distributions. LSGAN uses squared-error loss as an alternative to cross-entropy, and Mao et al. (2017) motivate this by noting that squared-error loss typically leads to sharper gradients.

Similar to an ideal standard GAN, the optimal discriminator losses of ideal WGAN and LSGAN are known constants—see the last column of Table 1 (these constants are derived by plugging $\mathbb{P}_g = \mathbb{P}_r$ in the discriminator loss).

2.1.1 Correlation between the Optimality Gap and Sample Quality

For all the GAN formulations in Table 1, it is known in theory that if the model capacity is sufficiently high, solving the optimization problem to global optimality leads to an ideal GAN (Goodfellow et al., 2014; Arjovsky et al., 2017; Mao et al., 2017). However, in practice, the capacity of the GAN is limited and optimization is done using first-order methods, which are generally not guaranteed to obtain optimal solutions. Thus, obtaining an ideal GAN in practice

is generally infeasible. However, as we demonstrate in our experiments, it is possible to train GANs that are “close enough” to an ideal GAN in terms of the loss. Specifically, given a GAN whose discriminator loss is \hat{V} , we define the *optimality gap* as $|\hat{V} - V^*|$. Our main hypothesis is:

GANs that achieve smaller optimality gaps tend to generate better samples.

We stress that this hypothesis applies to GANs that are trained with reasonable hyperparameters and initialization. It is possible to obtain GANs whose optimality gap is 0 or close to 0 without training, e.g., initializing a GAN with all-zero weights will lead to a 0 gap in standard GAN.

Empirical Evidence. We validate the hypothesis through multiple experiments on MNIST (Xiao et al., 2017), Fashion MNIST (Xiao et al., 2017), CIFAR-10 (Krizhevsky et al., 2009), and CelebA (Liu et al., 2015). Next, we briefly discuss one of these experiments and leave the rest to Section 4. We consider generating images from MNIST using a GAN, based on the DCGAN architecture (Radford et al., 2016), and we study different GAN variants (NSGAN, LSGAN, and WGAN). We consider 100 sets of hyperparameter values, drawn randomly, on which we train each GAN (see Section 4 for more details). For evaluation, we compute the Frechet Inception Distance (FID) (Heusel et al., 2017), which is a standard for assessing image quality.

In Figure 1, we present scatter plots of FID versus the optimality gap; here each point corresponds to a particular hyperparameter configuration. For the three variants of GAN, we observe medium to strong, positive spearman’s correlation between FID and the optimality gap. That is, models with a smaller optimality gap tend to have better image quality. The scheduler we develop (in Sec. 3) attempts to keep the optimality gap in check by modifying the learning rate.

2.2 Domain Adversarial Neural Nets (DANN)

DANN is another important example of adversarial nets used in domain adaptation (Ganin et al., 2016). Given labelled data from a source domain and unlabelled data from a related, target domain, the goal is to train a model that generalizes well on the target. The main principle behind DANN is that for good generalization, the feature representations should be domain-independent (Ben-David et al., 2010). DANN consists of: (i) a feature extractor F that receives features (from either the source or target data) and generates representations, (ii) a label predictor Y that classifies the source data based on the representations from the feature extractor, (iii) a discriminator D —a probabilistic classifier—that takes the feature representations from the extractor and attempts to predict whether the sample came from the source or target domain. Let \mathbb{P}_s and \mathbb{P}_t be the input distributions of the source and target domains, respectively.

Table 1: Popular GAN variations considered in this work. Both the discriminator and generator losses are minimized. The value V^* denotes the loss of the discriminator in an ideal GAN.

GAN	DISCRIMINATOR LOSS (MINIMIZED)	GENERATOR LOSS (MINIMIZED)	IDEAL DISCRIMINATOR LOSS V^*
STANDARD	$-\mathbb{E}_{x \sim \mathbb{P}_r} [\log(D(x))] - \mathbb{E}_{\tilde{x} \sim \mathbb{P}_g} [\log(1 - D(\tilde{x}))]$	$\mathbb{E}_{\tilde{x} \sim \mathbb{P}_g} [\log(1 - D(\tilde{x}))]$	$\log(4)$
NSGAN	$-\mathbb{E}_{x \sim \mathbb{P}_r} [\log(D(x))] - \mathbb{E}_{\tilde{x} \sim \mathbb{P}_g} [\log(1 - D(\tilde{x}))]$	$-\mathbb{E}_{\tilde{x} \sim \mathbb{P}_g} [\log(D(\tilde{x}))]$	$\log(4)$
WGAN	$-\mathbb{E}_{x \sim \mathbb{P}_r} [D(x)] + \mathbb{E}_{\tilde{x} \sim \mathbb{P}_g} [D(\tilde{x})]$	$-\mathbb{E}_{\tilde{x} \sim \mathbb{P}_g} [D(\tilde{x})]$	0
LSGAN	$\mathbb{E}_{x \sim \mathbb{P}_r} [(D(x) - 1)^2] + \mathbb{E}_{\tilde{x} \sim \mathbb{P}_g} [D(\tilde{x})^2]$	$\mathbb{E}_{\tilde{x} \sim \mathbb{P}_g} [(D(\tilde{x}) - 1)^2]$	0.5

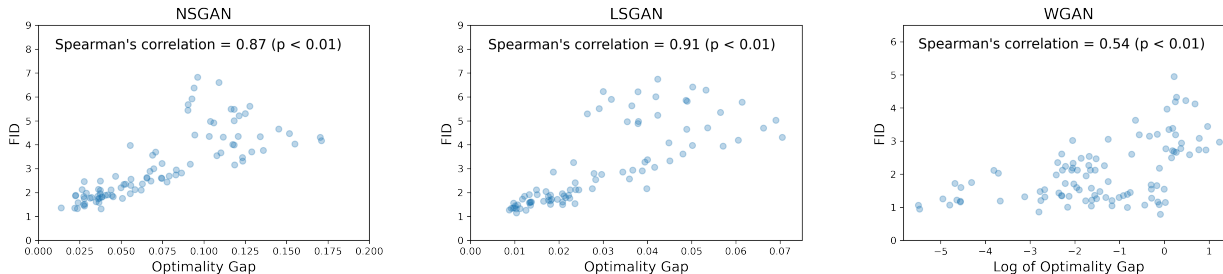


Figure 1: Scatter plots of the Frechet Inception Distance (FID) versus the optimality gap on MNIST. Each point corresponds to a particular hyperparameter configuration obtained by random sampling. Lower FID values typically correspond to better image quality. For the three GAN variants, we observe moderate to strong, positive (rank) correlation between FID and the optimality gap. To improve visualization, a small number of outliers was removed—these outliers do not affect correlation and are presented in Appendix A. For WGAN, we removed outliers with $FID > 5$ and applied a log transformation to the gap (since it varies over 8 orders of magnitude).

At the population level, DANN solves:

$$\min_{F, Y} \max_D \mathcal{L}_y(F, Y) - \lambda \mathcal{L}_d(F, D),$$

where $\mathcal{L}_y(F, Y)$ is the risk of the label predictor, λ is a non-negative hyperparameter, and $\mathcal{L}_d(F, D)$ is the discriminator risk defined by:

$$-\mathbb{E}_{x \sim \mathbb{P}_s} \log [D(F(x))] - \mathbb{E}_{\tilde{x} \sim \mathbb{P}_t} \log [1 - D(F(\tilde{x}))].$$

We say that DANN is ideal if the distribution of $F(x)$, $x \sim \mathbb{P}_s$ is the same as that of $F(\tilde{x})$, $\tilde{x} \sim \mathbb{P}_t$. By the same reasoning used for standard GAN, the optimal discriminator in this ideal case outputs 0.5, and thus $\mathcal{L}_d(F, D) = \log(4)$. However, generally, λ controls the extent to which the two distributions discussed above are matched, and thus the optimal $\mathcal{L}_d(F, D)$ generally depends on λ . Very small values of λ may⁵ lead to a discriminator that distinguishes well between the two domains. On the other hand, by increasing λ , we can get arbitrarily close the ideal case (where the discriminator outputs 0.5). In theory, for effective domain transfer, λ needs to be chosen large enough so that discriminator is well fooled (Ben-David et al., 2010), so for such λ 's we expect the optimal $\mathcal{L}_d(F, D)$ to be roughly close to $\log(4)$. Finally, similar to GANs, we remark that the ideal case is typically infeasible to achieve in practice (due to several factors, including using first-order methods and

⁵Small values are not always guaranteed to lead to a discriminator that distinguishes well. This depends on a combination of factors including the architecture and the input distributions. As a trivial example, if DANN is supplied with identical domains ($\mathbb{P}_s = \mathbb{P}_t$), the optimal discriminator outputs 0.5 for any $\lambda \geq 0$.

limited capacity); but controlling the optimality gap can be useful, as we demonstrate in our experiments.

3 Gap-Aware Learning Rate Scheduling

In Section 2, we presented empirical evidence that validates our hypothesis that GANs with smaller optimality gaps tend to generate higher quality samples. In this section, we put the hypothesis into action and design a learning rate scheduler that attempts to keep the gap relatively small throughout training. Besides the hypothesized improvement in sample quality, keeping the optimality gap small throughout training can mitigate potential drifts in the loss (e.g., the discriminator loss dropping towards zero), which may lead to more stable training. Next, we describe the optimization setup and then introduce the scheduling algorithm.

Optimization Setup. We assume that the optimization problem of the adversarial net is cast as a minimization over both the loss of the adversary D (e.g., the discriminator in a GAN) and the loss of the competing network G (e.g., the generator in a GAN). We focus on the popular strategy of optimizing the two competing networks simultaneously using (minibatch) SGD⁶. We use the notation α_d to refer to the learning rate of D . The learning rate scheduler will modify α_d throughout training whereas the learning rate of G remains fixed. We note that the scheduler can be applied to adaptive optimizers (e.g., Adam or RMSProp) as well—in such cases, α_d will refer to the base learning rate. We denote

⁶This is SGDA if optimization over D is formulated as maximization.

by V_d the current loss of D (a scalar representing the average of the loss over the whole training data). The scheduler takes V_d and D 's ideal loss V^* as inputs and outputs a scalar, which is used as a multiplier to adjust α_d .

Effect of D 's learning rate on the optimality gap. Recall that in our setup D and G are simultaneously optimized. During each optimizer update, D aims to decrease V_d while G typically aims to increase V_d . The optimizer update may increase or decrease V_d , depending on how large D 's learning rate is w.r.t. that of G . If D 's learning rate is sufficiently larger, we expect V_d to decrease after the update, and otherwise, we expect V_d to increase. This intuition will be the basis of how the scheduler controls the optimality gap.

Next, we introduce the scheduling mechanism, where we differentiate between two cases: **(i)** $V_d \geq V^*$ and **(ii)** $V_d < V^*$.

Scheduling when $V_d \geq V^*$. First, we give an abstract definition of the scheduler and then define the scheduling function formally. In this case, the current loss of D is larger than V^* , so to reduce the gap, we need to decrease V_d . As discussed earlier, this effect can be achieved by increasing D 's learning rate sufficiently. Therefore, when $V_d \geq V^*$, we design the scheduler to increase the learning rate, and we make the increase proportional to the gap ($V_d - V^*$), so that the scheduler focuses more on larger deviations from optimality.

There are a couple of important constraints that should be taken into account when increasing the learning rate. First, the increase should be bounded because too large of a learning rate will lead to convergence issues. Second, we need to control the rate of increase and ensure the chosen rate works in practice (e.g., too fast of a rate can lead to sharp changes in the loss and cause instabilities). Next, we define a function that satisfies the desired constraints.

We introduce a scheduling function $f : \mathbb{R} \rightarrow \mathbb{R}$, which takes $x := (V_d - V^*)$ as an input and returns a multiplier for the learning rate. That is, the new learning rate of the discriminator (after scheduling) will be $\alpha_d \times f(x)$. To satisfy the constraints discussed above (boundedness and rate control), we introduce two user-specified parameters: $f_{\max} \in [1, \infty)$ and $x_{\max} \in \mathbb{R}_{>0}$. The function f interpolates between the points $(0, 1)$ and (x_{\max}, f_{\max}) and caps at f_{\max} , i.e., $f(x) = f_{\max}$ for $x \geq x_{\max}$. Here x_{\max} is viewed as a parameter that controls the rate of the increase—a larger x_{\max} leads to a slower rate, and thus the scheduler becomes less stringent. There are different possibilities for interpolation. In our experiments, we tried linear and exponential interpolation and found the latter to work slightly better. Thus, we use exponential interpolation and define f as:

$$f(x) = \min \left\{ [f_{\max}]^{x/x_{\max}}, f_{\max} \right\}. \quad (1)$$

Note that since $f_{\max} \geq 1$, we always have $f(x) \geq 1$ for

$x \geq 0$, so the learning rate will increase after scheduling. Moreover, the learning rate is not modified when the gap is zero since $f(0) = 1$.

Scheduling when $V_d \leq V^*$. In this case, reducing the gap requires increasing V_d . This can be achieved by decreasing the learning rate of D . Similar to the previous case, we design the scheduler so that the decrease is proportional to $(V^* - V_d)$ (a non-negative quantity). More formally, we define a scheduling function $h : \mathbb{R} \rightarrow \mathbb{R}$, which takes $x := (V^* - V_d)$ as an input and returns a multiplier for the learning rate, i.e., the new learning rate is $\alpha_d \times h(x)$. Similar to the previous case, we introduce two user-specified parameters $h_{\min} \in (0, 1]$ (the minimum value h can take) and $x_{\min} \in \mathbb{R}_{>0}$ to control the decay rate. We define h as an interpolation between $(0, 1)$ and (x_{\min}, h_{\min}) , which is clipped from below at h_{\min} . We use exponential decay interpolation, leading to:

$$h(x) = \max \left\{ [h_{\min}]^{x/x_{\min}}, h_{\min} \right\}. \quad (2)$$

Since $h_{\min} \in [0, 1]$, we always have $h(x) \leq 1$ for $x \geq 0$, implying that the learning rate will decrease after scheduling. We summarize the scheduling mechanism in Algorithm 1.

Algorithm 1: Gap-Aware Scheduling Algorithm

Inputs: Current loss V_d and ideal loss V^* .

Parameters: $x_{\min}, x_{\max}, h_{\min} \in (0, 1], f_{\max} \in [1, \infty)$.

1. If $V_d \geq V^*$, increase D 's learning rate by multiplying it with $f(V_d - V^*)$ – see (1).
2. If $V_d < V^*$, decrease D 's learning rate by multiplying it with $h(V^* - V_d)$ – see (2).

In our experiments, we inspect the optimality gap of GANs trained with and without the scheduler. We observe that the scheduler effectively reduces the optimality gap on all datasets and GAN variants, by up to 70x (see Table 2). In most cases, we also observe that models with smaller gaps tend to have better sample quality.

Choice of Parameters. Based on our experiments, we propose setting the same base learning rate for G and D (and tuning over the learning rate, if the computational budget allows). Under this setting, in all of our GAN experiments and across all datasets, we fix the parameters: $h_{\min} = 0.1$, $f_{\max} = 2$, $x_{\min} = x_{\max} = 0.1V^*$ for NSGAN and LSGAN; and $x_{\min} = x_{\max} = 0.1$ for WGAN. These values were only tuned on MNIST for a very limited number of configurations—see Appendix B for details and intuition. We found these parameters to transfer well to Fashion MNIST, CIFAR-10, and CelebA. In Section 4, we present a sensitivity analysis in which we vary these parameters over multiple orders of magnitude. The results generally indicate that the

scheduler is relatively stable around the default values reported above (but setting these parameters to extreme values may cause instabilities).

For the DANN experiments, we use the same fixed parameters as in GANs ($x_{\max} = x_{\min} = 0.1V^*$), but we consider a single tuning parameter: V^* . As discussed in Section 2.2, the optimal discriminator loss in DANN depends on λ , but we expect it to be roughly close to $\log(4)$ (for good choices of λ). In our experiments we tune over $V^* \in [0.5 \log(4), \log(4)]$ and demonstrate that DANN is not sensitive to V^* , e.g., with only 10 random search trials for tuning the base learning rate, V^* , and λ , optimizing with the scheduler outperforms its no-scheduler counterpart (with the same tuning budget).

Batch-level Scheduling. We apply Algorithm 1 at the batch level, i.e., the learning rate is modified at each minibatch update. The motivation behind batch-level scheduling is to keep the loss in check after each update. One popular alternative is to schedule at the epoch level. However, if the epoch involves many batches, the loss may drift drastically throughout one or few epochs (an observation that is common in practice). Scheduling at the batch level can mitigate such drifts early on.

Estimating the Current Discriminator Loss. The scheduling algorithm requires access to the discriminator’s loss V_d at every minibatch update. The loss should be ideally evaluated over all training examples, however, this is typically inefficient. We resort to an exponential moving average to estimate V_d . Specifically, let \hat{V}_d be the current estimate of V_d and denote by V_{batch} the loss of the current batch (which is available from the forward pass). The moving average update is: $\hat{V}_d \leftarrow \alpha \hat{V}_d + (1 - \alpha)V_{\text{batch}}$, where $\alpha \in [0, 1)$ is a user-specified parameter that controls the decay rate. In all experiments, we fix $\alpha = 0.95$ (no tuning was performed) and initialize with V^* . We also note that if the training loss is evaluated periodically over the whole dataset (e.g., every number of epochs), the moving average can be reinitialized with this value.

4 Experiments

We study the performance of the scheduler on GANs for image generation and DANN.

4.1 GANs

GANs are generally sensitive to weight initialization and hyperparameters (especially, learning rate) and require sufficiently large tuning budgets to perform well (Lucic et al., 2018). Thus, our main goal is to study if the learning rate scheduler can improve stability and reduce the need for tuning.

A Statistical Study. We perform a systematic study in

which we tune GANs under different tuning budgets and repeat experiments over many random seeds. Our study allows for a rigorous understanding of the statistical significance and stability of the results. The study is large-scale as it involves training over 25,000 GANs (for 100s of epochs each) and requires around 6 GPU years on NVIDIA P100. In this respect, we note that a large part of the literature on GANs reports results on a single random seed and manually tunes hyperparameters (without reporting the tuning budget)—as reported by Lucic et al. (2018), this may result in misleading conclusions.

Competing Methods, Datasets, and Architecture. We compare with popular mechanisms for choosing the learning rate, including using the same learning rate for G and D , decoupled learning rates (tuned independently) (Heusel et al., 2017), and a classical scheduler that monotonically decays the learning rate. Since our study involves training a large number of GANs (over 25,000), we consider the following standard datasets that allow for reasonable computation time: CelebA, CIFAR, Fashion MNIST, and MNIST. We focus on three popular GAN variants: NSGAN, LSGAN, and WGAN, and use a DCGAN architecture (Radford et al., 2016)—see Appendix D for details. Our setup (both datasets and architecture) is standard for large-scale tuning studies of GANs, e.g., see Lucic et al. (2018).

While it would be interesting to consider larger datasets and architectures, we note that performing such a large-scale study may become computationally infeasible. Moreover, we stress that our goal is to understand how the scheduler performs compared to other alternatives, under a clear, fixed tuning budget. Thus, it would be unfair to compare with models in the literature that do not report the tuning budget and the exact tuning procedure.

Experimental Details. We use Adam (Kingma and Ba, 2015) as it is the most popular choice for optimizing GANs (Wang et al., 2021), and fix the batch size to 256. On MNIST, Fashion MNIST, and CIFAR, we use 500 epochs, and 200 epochs on CelebA (as it is $\sim 3x$ larger than the other datasets). To avoid overfitting, we periodically compute FID on the validation set during training, and upon termination return the version of the model with the best FID (this simulates early stopping). We tune over the following key hyperparameters: base learning rate(s), β_1 in Adam, and the clipping weight in WGAN. We consider two settings when tuning the base learning rate: (i) the same rate for both G and D , and (ii) two decoupled rates that are tuned independently (Heusel et al., 2017). We report the results of (i) in the main paper and the results of (ii) in the appendix—in both cases, the scheduler outperforms its no scheduler counterpart. We use 100 trials of random search, where in each trial, training is repeated 5 times over random seeds to reduce variability. We use FID on the validation set as the tuning metric, and we report the final FID results on a separate test set. See Appendix D for more details.

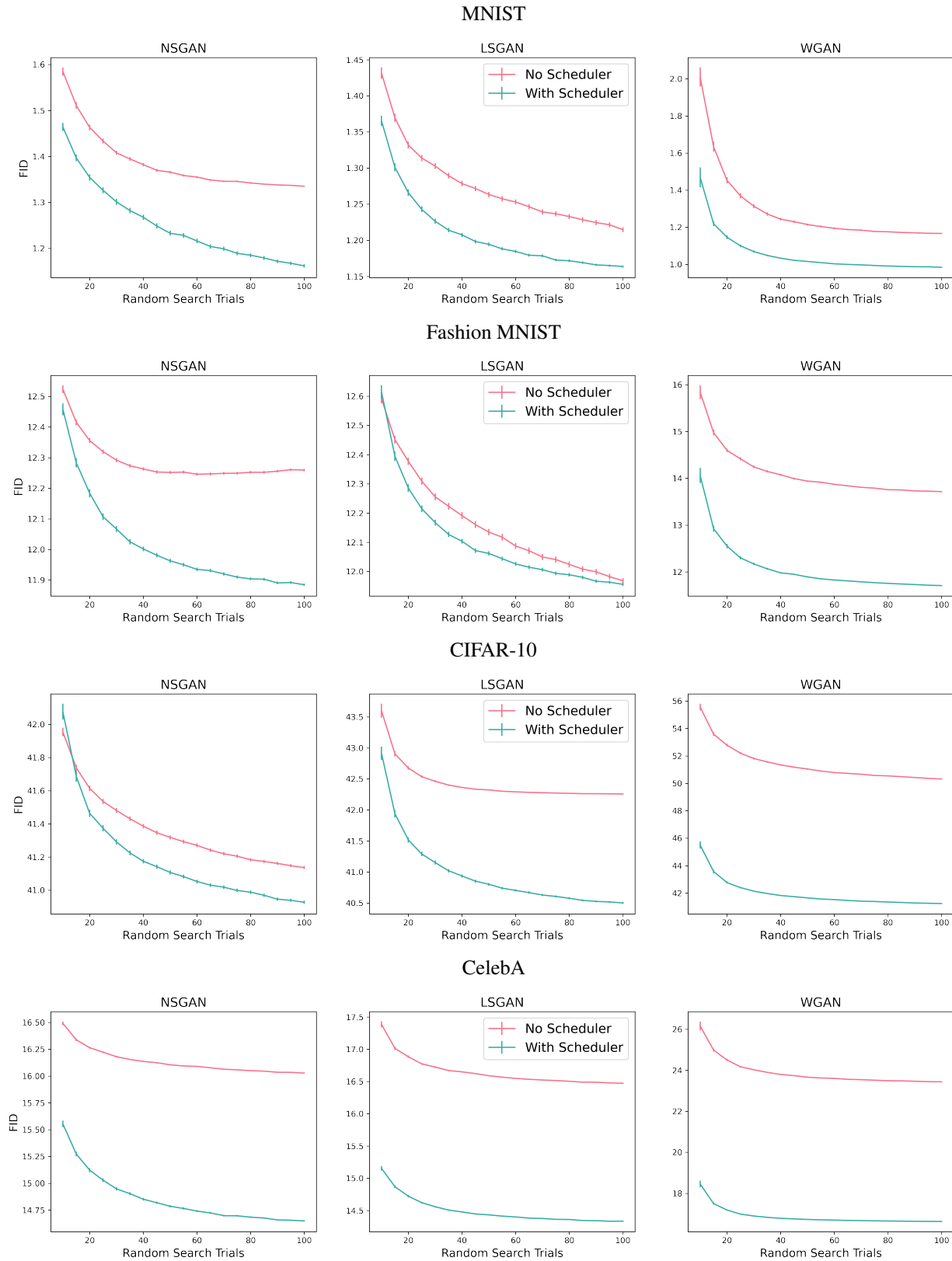


Figure 2: Plots of the best FID as function of the tuning budget. Following Lucic et al. (2018), for each tuning budget k , we report the mean and 99% confidence intervals of the best FID, estimated using 5,000 bootstrap samples of size k from the original 100 tuning runs.

Table 2: Frechet Inception Distance (lower is better), Inception Score (higher is better), and the Optimality Gap (multiplied by 10^3) on the test set after tuning. Each entry represents the mean and standard error, computed over 100 training runs (initialized with random seeds). Best values are in bold. An asterisk (*) indicates statistical significance based on a two-sample t-test at a level of 0.01.

GAN/Dataset	FID				Inception Score				Optimality Gap $\times 10^3$			
	MNIST	Fashion	CIFAR	CelebA	MNIST	Fashion	CIFAR	CelebA	MNIST	Fashion	CIFAR	CelebA
NS	1.4 (0.03)	12.4 (0.04)	42.1 (0.09)	16.5 (0.06)	8.18 (0.01)	4.11 (0.01)	6.27 (0.01)	3.1 (0.01)	22 (1)	34 (1)	203 (6)	513 (8)
NS + Sched.	1.2 (0.02)*	12.0 (0.04)*	41.1 (0.1)*	15.0 (0.07)*	8.23 (0.01)*	4.11 (0.01)	6.41 (0.01)*	3.12 (0.0004)	19 (1)	34 (1)	91 (3)*	238 (5)
LS	1.3 (0.02)	12.2 (0.04)	68.1 (10.28)	40.6 (9.5)	8.19 (0.01)	4.04 (0.03)	6.01 (0.13)	2.97 (0.05)	10 (1)	17 (0.4)	115 (10)	246 (8)
LS + Sched.	1.3 (0.02)	12.1 (0.04)	40.9 (0.09)*	14.5 (0.05)*	8.19 (0.01)	4.11 (0.01)	6.4 (0.01)*	3.12 (0.0004)	11 (1)	17 (0.4)	27 (0.4)*	111 (3)*
W	1.1 (0.02)	13.8 (0.06)	49.9 (0.11)	23.4 (0.11)	8.32 (0.01)	4.1 (0.01)	5.93 (0.01)	2.99 (0.01)	2143 (169)	346 (35)	11801 (813)	9861 (225)
W + Sched.	1.0 (0.02)*	11.6 (0.04)*	41.8 (0.17)*	17.1 (0.11)*	8.4 (0.01)*	4.15 (0.01)*	6.32 (0.02)*	3.1 (0.01)	57 (5)*	117 (9)*	825 (96)*	139 (6)*

4.1.1 Results

Tuning Budget and Performance. Here we compare the performance with and without the scheduler, using the same base learning rate for G and D ; see Appendix C for decoupled rates (Heusel et al., 2017). In Figure 2, we plot the best FID as a function of the tuning budget. The results indicate that on all datasets, all variants of GANs, and almost every computational budget, the scheduler outperforms the (tuned) optimizer without the scheduler. The improvement reaches up to 27% in some cases, e.g., for WGAN on CelebA. The magnitude of the improvement is more pronounced on CelebA and CIFAR compared to MNIST/Fashion MNIST. This may be attributed to the more complex nature of CelebA and CIFAR, which can require more careful choices of the learning rates. Additionally, we note that the learning rate with the scheduler does not monotonically decrease (as in common learning rate decay)—it varies up and down as the training progresses (see Figure C.2 in the appendix).

Stability. To get an idea about the stability of the scheduler w.r.t. weight initialization, we pick the best hyperparameters from the tuning study (after 100 random search trials), and train each model 100 times using random seeds. In Table 2, we report the mean and standard error of both FID and the Inception Score (Salimans et al., 2016). The improvements we saw from using the scheduler in the tuning study (represented by Figure 2) generalize to this experiment, i.e., the performance of the scheduler does not seem to be sensitive to the random seed. For LSGAN *without* the scheduler, there are significant outlier runs (the standard error is ~ 10) on CIFAR-10 and CelebA—the same observation was made by Lucic et al. (2018) for LSGAN on the latter datasets. In contrast, for LSGAN with the scheduler, we did not observe outlier runs and this is evidenced by the small standard error (< 0.1). Thus, for the datasets considered, the scheduler appears to be generally more stable.

Optimality Gap. In Table 2, we also report the optimality gap of the tuned models (averaged over 100 randomly initialized training runs). Out of the 12 dataset/GAN-type pairs, the scheduler achieves a strictly lower optimality gap

in 9 cases, equal gap in 2 cases, and 1 worse gap that is statistically insignificant (see LSGAN on MNIST). On CIFAR and CelebA, the scheduler achieves significantly lower gaps, e.g., 70x lower for WGAN on CelebA. For LSGAN on MNIST and Fashion MNIST, the optimizer without the scheduler already achieves small gaps, so the scheduler does not offer noticeable improvements. Generally, the results are in line with our hypothesis that models with smaller optimality gaps tend to generate better samples.

Sensitivity Analysis. We study the sensitivity of the scheduler to its parameters: h_{\min} , f_{\max} , x_{\min} , and x_{\max} . Specifically, we vary the value of each parameter (individually) over multiple orders of magnitude and study the change in FID. When varying a given parameter, we fix the other parameters to their default values (discussed in Section 3). The analysis is done on MNIST using the best (tuned) hyperparameters of the GAN, and training is repeated for 50 random seeds to account for the variability due to initialization. In Figure 3, we present sensitivity plots for NSGAN, LSGAN, and WGAN.

The results indicate that NSGAN and WGAN are relatively insensitive: there is a wide range of values (over one order of magnitude) that lead to good performance, which exceeds that of no scheduler. LSGAN has sharp transitions for large values of f_{\max} (specifically > 5); this is intuitively expected because increasing the learning rate beyond a certain threshold will cause the model to diverge. For very small x_{\min} and x_{\max} (< 0.02), LSGAN performs poorly; this is also expected because such small values force the training loss to be almost constant so essentially the model does not train. We also note that LSGAN is known in the literature to be more sensitive and suffer from frequent failure even for well-tuned hyperparameters, compared to NSGAN and WGAN (Lucic et al., 2018).

Optimality Gap of G. Given that the scheduler only controls the learning rate (and loss) of D , a natural question is: what happens to the loss of G ? In Appendix C, we study the effect of the scheduler on G 's loss. Specifically, we measure G 's optimality gap, which we define as the absolute difference between G 's training and ideal losses. The main conclusion of the experiment is that the scheduler

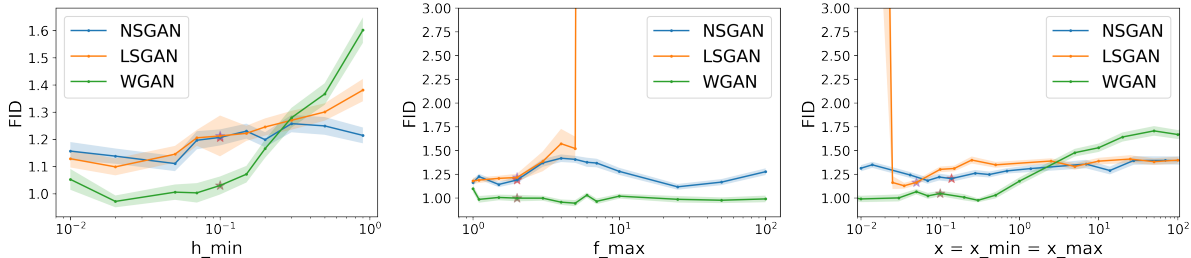


Figure 3: Sensitivity plots for the scheduler applied to NSGAN, LSGAN, and WGAN on MNIST. The x-axis is on a log scale. When varying each parameter, we fix the other parameters to the default values. We repeat training 50 times (using random seeds) and report the mean and standard error (represented by the shaded region). A star represents the default parameter value used in the experiments.

can significantly reduce G 's optimality gap, compared to no scheduler.

Additional Comparisons. In Appendix C, we compare with two additional alternative strategies for choosing the learning rate: (i) decoupled base learning rates (tuned independently) (Heusel et al., 2017), and (ii) a classical scheduler that monotonically decreases the learning rate. In both cases, the scheduler reduces the need for tuning (by up to 10x) and significantly improves FID (by up to 38%). Moreover, we present a comparison between exponential and linear interpolation for the scheduling functions $f(x)$ and $h(x)$.

4.2 DANN

We consider a standard domain adaptation benchmark: MNIST as the source and MNIST-M as the target. MNIST-M consists of MNIST images whose background has been altered (Ganin et al., 2016). We conduct a tuning study to understand how DANN with the scheduler compares to (i) DANN without a scheduler and (ii) a model without domain adaptation (i.e., trained only on the source).

Experimental Setup. We use a CNN-based architecture for DANN, similar to that in Ganin and Lempitsky (2015), and optimize using SGD with a batch size of 256. We train for 300 epochs, computing the validation accuracy at each epoch. At the end of training, we pick the version of the model with the highest validation accuracy (simulating early stopping). Additionally, we tune over the following hyperparameters: learning rate, λ , and V^* , using 100 random search trials, and training is repeated 5 times per trial (using random seeds). See Appendix D for details.

Results. In Figure 4 (left), we report the test accuracy (on the target) as a function of the tuning budget for DANN with and without the scheduler. The results indicate that the scheduler performs better for every tuning budget. The relative improvement in mean accuracy reaches around 0.7% at 100 trials. We also experimented with a source-only model that does not perform domain adaptation (specifi-

cally, DANN with $\lambda = 0$). The accuracy of the source-only model is 60.4% (with standard error of 0.4%) at 100 trials, which is significantly lower than the two models in Figure 4. In Figure 4 (right), we study the training stability of the model using the optimal hyperparameters (obtained by tuning). Specifically, we report the accuracy of 100 models trained with random initialization. We observe that the scheduler has roughly a 40% smaller interquartile range, suggesting that it leads to more stable training. Moreover, the scheduler significantly improves the lower tail of the accuracy distribution, e.g., the first quartile and minimum (worst-case) accuracy improve by 1% and 3%, respectively.

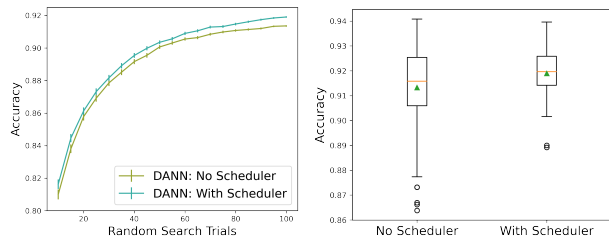


Figure 4: Domain adaptation (MNIST \rightarrow MNIST-M) using DANN. **[Left]** Test accuracy of the best model as a function of the tuning budget. The 99% confidence intervals are estimated using 5000 bootstrap samples. **[Right]** Training stability: test accuracy of 100 models trained using random initialization and optimal hyperparameters.

5 Conclusion

We proposed a novel gap-aware learning rate scheduler for adversarial nets. The scheduler monitors the optimality gap (from an ideal network) during training and modifies the base learning rate to keep the gap in check. This is in contrast to the common choices of base learning rates which do not take into account the gap or the current state of the network. Our experiments on GANs for image generation and DANN for domain adaptation demonstrate that the scheduler can significantly improve performance and reduce the need for tuning.

References

- Abadi, M., Agarwal, A., Barham, P., Brevdo, E., Chen, Z., Citro, C., Corrado, G. S., Davis, A., Dean, J., Devin, M., Ghemawat, S., Goodfellow, I., Harp, A., Irving, G., Isard, M., Jia, Y., Jozefowicz, R., Kaiser, L., Kudlur, M., Levenberg, J., Mané, D., Monga, R., Moore, S., Murray, D., Olah, C., Schuster, M., Shlens, J., Steiner, B., Sutskever, I., Talwar, K., Tucker, P., Vanhoucke, V., Vasudevan, V., Viégas, F., Vinyals, O., Warden, P., Wattenberg, M., Wicke, M., Yu, Y., and Zheng, X. (2015). TensorFlow: Large-scale machine learning on heterogeneous systems. Software available from tensorflow.org.
- Abadi, M. and Andersen, D. G. (2016). Learning to protect communications with adversarial neural cryptography. *arXiv preprint arXiv:1610.06918*.
- Arjovsky, M., Chintala, S., and Bottou, L. (2017). Wasserstein generative adversarial networks. In *International conference on machine learning*, pages 214–223. PMLR.
- Ben-David, S., Blitzer, J., Crammer, K., Kulesza, A., Pereira, F., and Vaughan, J. W. (2010). A theory of learning from different domains. *Machine learning*, 79(1):151–175.
- Che, T., Li, Y., Jacob, A. P., Bengio, Y., and Li, W. (2017). Mode regularized generative adversarial networks. In *5th International Conference on Learning Representations, ICLR 2017*.
- Ganin, Y. and Lempitsky, V. (2015). Unsupervised domain adaptation by backpropagation. In *International conference on machine learning*, pages 1180–1189. PMLR.
- Ganin, Y., Ustinova, E., Ajakan, H., Germain, P., Larochelle, H., Laviolette, F., Marchand, M., and Lempitsky, V. (2016). Domain-adversarial training of neural networks. *The journal of machine learning research*, 17(1):2096–2030.
- Goodfellow, I., Pouget-Abadie, J., Mirza, M., Xu, B., Warde-Farley, D., Ozair, S., Courville, A., and Bengio, Y. (2014). Generative adversarial nets. *Advances in neural information processing systems*, 27.
- Gulrajani, I., Ahmed, F., Arjovsky, M., Dumoulin, V., and Courville, A. (2017). Improved training of wasserstein gans. In *Proceedings of the 31st International Conference on Neural Information Processing Systems*, pages 5769–5779.
- Heusel, M., Ramsauer, H., Unterthiner, T., Nessler, B., and Hochreiter, S. (2017). Gans trained by a two time-scale update rule converge to a local nash equilibrium. *Advances in neural information processing systems*, 30.
- Karras, T., Aittala, M., Hellsten, J., Laine, S., Lehtinen, J., and Aila, T. (2020). Training generative adversarial networks with limited data. In *IEEE Conference on Neural Information Processing Systems*.
- Kingma, D. P. and Ba, J. (2015). Adam: A method for stochastic optimization. In Bengio, Y. and LeCun, Y., editors, *3rd International Conference on Learning Representations, ICLR 2015, San Diego, CA, USA, May 7-9, 2015, Conference Track Proceedings*.
- Krizhevsky, A., Hinton, G., et al. (2009). Learning multiple layers of features from tiny images.
- Lee, K., Chang, H., Jiang, L., Zhang, H., Tu, Z., and Liu, C. (2021). Vitgan: Training gans with vision transformers. *arXiv preprint arXiv:2107.04589*.
- Li, C.-L., Chang, W.-C., Cheng, Y., Yang, Y., and Póczos, B. (2017). Mmd gan: towards deeper understanding of moment matching network. In *Proceedings of the 31st International Conference on Neural Information Processing Systems*, pages 2200–2210.
- Li, Y., Swersky, K., and Zemel, R. S. (2015). Generative moment matching networks. In Bach, F. R. and Blei, D. M., editors, *Proceedings of the 32nd International Conference on Machine Learning, ICML 2015, Lille, France, 6-11 July 2015*, volume 37 of *JMLR Workshop and Conference Proceedings*, pages 1718–1727. JMLR.org.
- Liu, Z., Luo, P., Wang, X., and Tang, X. (2015). Deep learning face attributes in the wild. In *Proceedings of International Conference on Computer Vision (ICCV)*.
- Lucic, M., Kurach, K., Michalski, M., Gelly, S., and Bousquet, O. (2018). Are gans created equal? A large-scale study. In Bengio, S., Wallach, H. M., Larochelle, H., Grauman, K., Cesa-Bianchi, N., and Garnett, R., editors, *Advances in Neural Information Processing Systems 31: Annual Conference on Neural Information Processing Systems 2018, NeurIPS 2018, December 3-8, 2018, Montréal, Canada*, pages 698–707.
- Mao, X., Li, Q., Xie, H., Lau, R. Y., Wang, Z., and Paul Smolley, S. (2017). Least squares generative adversarial networks. In *Proceedings of the IEEE international conference on computer vision*, pages 2794–2802.
- Mescheder, L., Geiger, A., and Nowozin, S. (2018). Which training methods for gans do actually converge? In *International conference on machine learning*, pages 3481–3490. PMLR.
- Mescheder, L., Nowozin, S., and Geiger, A. (2017). The numerics of gans. In *Proceedings of the 31st International Conference on Neural Information Processing Systems*, pages 1823–1833.
- Nagarajan, V. and Kolter, J. Z. (2017). Gradient descent gan optimization is locally stable. In *Proceedings of the 31st International Conference on Neural Information Processing Systems*, pages 5591–5600.
- Neyshabur, B., Bhojanapalli, S., and Chakrabarti, A. (2017). Stabilizing gan training with multiple random projections. *arXiv preprint arXiv:1705.07831*.

- Nowozin, S., Cseke, B., and Tomioka, R. (2016). f-gan: Training generative neural samplers using variational divergence minimization. In *Proceedings of the 30th International Conference on Neural Information Processing Systems*, pages 271–279.
- Radford, A., Metz, L., and Chintala, S. (2016). Unsupervised representation learning with deep convolutional generative adversarial networks. In Bengio, Y. and LeCun, Y., editors, *4th International Conference on Learning Representations, ICLR 2016, San Juan, Puerto Rico, May 2-4, 2016, Conference Track Proceedings*.
- Razaviyayn, M., Huang, T., Lu, S., Nouiehed, M., Sanjabi, M., and Hong, M. (2020). Nonconvex min-max optimization: Applications, challenges, and recent theoretical advances. *IEEE Signal Processing Magazine*, 37(5):55–66.
- Salimans, T., Goodfellow, I., Zaremba, W., Cheung, V., Radford, A., and Chen, X. (2016). Improved techniques for training gans. *Advances in neural information processing systems*, 29:2234–2242.
- Wang, Z., She, Q., and Ward, T. E. (2021). Generative adversarial networks in computer vision: A survey and taxonomy. *ACM Computing Surveys (CSUR)*, 54(2):1–38.
- Xiao, H., Rasul, K., and Vollgraf, R. (2017). Fashion-mnist: a novel image dataset for benchmarking machine learning algorithms. *CoRR*, abs/1708.07747.
- Xu, K., Li, C., Zhu, J., and Zhang, B. (2020). Understanding and stabilizing gans’ training dynamics using control theory. In *International Conference on Machine Learning*, pages 10566–10575. PMLR.
- Yadav, A., Shah, S., Xu, Z., Jacobs, D., and Goldstein, T. (2018). Stabilizing adversarial nets with prediction methods. In *International Conference on Learning Representations*.
- Zhang, B. H., Lemoine, B., and Mitchell, M. (2018). Mitigating unwanted biases with adversarial learning. In *Proceedings of the 2018 AAAI/ACM Conference on AI, Ethics, and Society*, pages 335–340.
- Zhao, J., Mathieu, M., and LeCun, Y. (2017). Energy-based generative adversarial networks. In *5th International Conference on Learning Representations, ICLR 2017*.

A FID versus Optimality Gap

In Figure 1, we removed a small number of outlier points to improve visualization. Below we plot all points including outliers. These outliers have $< 1\%$ effect on Spearman’s correlation. For WGAN, a significant number of runs had $\text{FID} > 5$ (corresponding to failures), so we removed these and added additional (non-failing) training runs to have approximately 100 points in the final plot.

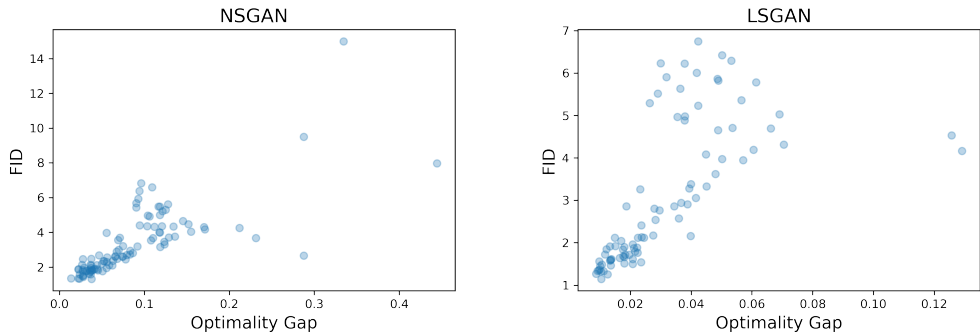


Figure A.1: Plots of FID vs. optimality gap for NSGAN and LSGAN with all outliers included.

B Scheduler’s Parameters

On MNIST, we tried a total of 8 configurations, which are the Cartesian product of: $h_{\min} \in \{0.5, 0.1\}$, $f_{\min} \in \{2, 10\}$, $x_{\min} = x_{\max} \in \{0.1V^*, 0.5V^*\}$ (V^* is dropped for WGAN). We found $h_{\min} = 0.1$, $f_{\max} = 2$, $x_{\min} = x_{\max} = 0.1V^*$ for NSGAN and LSGAN; and $x_{\min} = x_{\max} = 0.1$ for WGAN to work best. We noticed that setting $f_{\max} = 10$ can lead to instabilities—intuitively, there is an upper bound on the learning rate after which the model will diverge. For the opposite direction, i.e., when decreasing the learning rate, having a relatively low floor such as 0.1 (as opposed to 0.5) does not seem to cause instabilities (which is expected with small learning rates).

C Additional Experimental Results

Scheduler’s Output. In Figure C.2, we visualize the output of the scheduler (the multiplier of the learning rate) for NSGAN, LSGAN, and WGAN using the tuned hyperparameters. The results generally show that the learning rate multiplier continuously goes up and down during training (based on the current optimality gap).

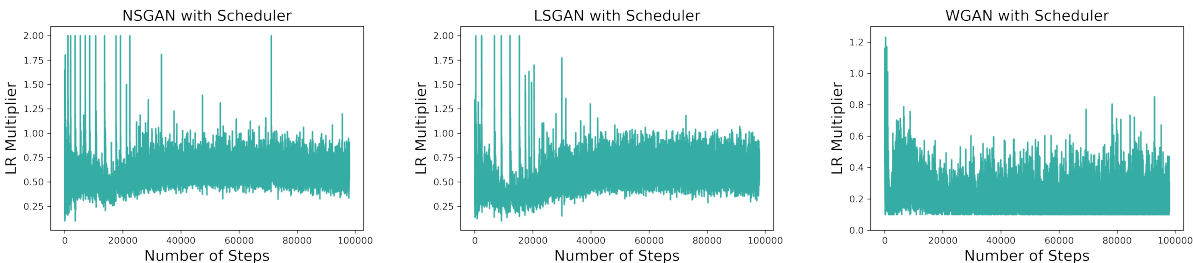


Figure C.2: Change in learning rate multiplier as the training progresses for NSGAN, LSGAN and WGAN with the scheduler, on MNIST. This demonstrates that the learning rate varies up and down during training.

Tuning Study for Decoupled (Different) Learning Rates. In Figure C.3, we report the results of the tuning study when the base learning rates of G and D are tuned independently. The results conform with the conclusions we had from the same-rate setting: the scheduler outperforms its no-scheduler counterpart for most tuning budgets.

Exponential Decay vs. Our Scheduler. In Figure C.4, we compare our scheduler versus a (classical) exponential decay scheduler that decays the learning rate monotonically (i.e., does not depend on the loss of the network), on MNIST. We

apply exponential decay at every step, in which the base learning rate is multiplied by $\rho^{s/T}$ where s is the index of the current step and T is the total number of steps. We tune both models (similar to the tuning experiment in the main paper), including the decay factor ρ which we sample from a log-uniform distribution over the range $[10^{-4}, 0.1]$.

Scheduling Function: Exponential vs. Linear Interpolation. Recall that we use exponential interpolation in the scheduling functions $f(x)$ and $h(x)$. Here we compare with linear interpolation, which is a natural alternative. For each interpolation method, we tune a GAN on MNIST, with the same architecture and tuning setup described in Section 4. Using the best hyperparameters, we then train the GAN 100 times (using random seeds) and report the test FID. We report the results for both interpolation methods in Table C.1. The results indicate that exponential interpolation performs slightly better than linear interpolation for all the three GAN types considered.

G’s Optimality Gap. While the scheduler is designed to control the learning rate (and consequently the gap) of D , we note that the scheduler also indirectly controls the optimality gap of G . Specifically, we define G ’s optimality gap as the absolute difference between G ’s training and ideal losses. G ’s ideal loss can be derived similar to that of D ; e.g., for NSGAN it is $\log(2)$. In Table C.2, we report G ’s optimality gap for GANs trained with and without the scheduler. The results indicate that the scheduler (which only controls D ’s LR) can significantly reduce G ’s optimality gap (by up to 60x).

Table C.1: Test FID of Exponential vs. Linear scheduling. We report the mean and standard error over 100 training runs (after tuning both).

	FID (smaller is better)	
	Exponential	Linear
NS + Sched.	1.23 (0.02)	1.26 (0.04)
LS + Sched.	1.29 (0.02)	1.33 (0.03)
W + Sched.	0.98 (0.02)	1.07 (0.02)

Table C.2: G ’s optimality gap (absolute difference between G ’s training and ideal losses) multiplied by 10^3 . We report the mean and standard error over 100 training runs. Our scheduler, which only controls D , significantly reduces the optimality gap of G , compared to no scheduler. Asterisk (*) means statistically significant based on a t-test at a level of 0.01.

GAN/Dataset	Generator’s Optimality Gap $\times 10^3$			
	MNIST	Fashion	CIFAR	CelebA
NS	90 (7)	55 (4)	308 (18)	994 (26)
NS + Sched.	76 (6)	48 (4)	155 (6)*	358 (9)*
LS	48 (4)	29 (2)	194 (0.01)	380 (0.007)
LS + Sched.	50 (4)	22 (2)	74 (1)*	145 (4)*
W	138685 (6771)	8065 (465)	16883 (491)	7141 (520)
W + Sched.	2320 (189)*	5211 (155)*	9597 (172)*	1612 (33)*

D Experimental Details

Computing Setup: We ran the experiments on a cluster equipped with P100 GPUs (we do not report the specs of the cluster for confidentiality). The tuning experiments took roughly 6 GPU years. All models were implemented and trained using TensorFlow 2 (Abadi et al., 2015), ran in GPU mode.

D.1 GANs

Datasets and Processing: For MNIST and Fashion MNIST, we use 50,000 examples for training, and 10,000 examples for each of the validation and test sets. For CIFAR, we use 40,000 examples for training, and 10,000 for each of the validation and test sets. For CelebA, we use the standard training set of 162,770 examples, and uniformly sample 10,000 examples for validation and testing from the standard validation/test sets, when computing FID. All pixels are rescaled to $[-1, 1]$, and for CelebA we resize all images to 32×32 (to reduce the memory requirements during training).

FID and Inception Score: FID and the Inception Score are computed using TF-GAN⁷ based on the Inception model, with the exception of MNIST, where TF-GAN uses a model trained on MNIST (with 99% accuracy). For both measures, we use 10,000 generated images, and additionally for FID we use 10,000 real images from either the validation or test sets (depending on whether the validation or test FID is being computed).

⁷<https://github.com/tensorflow/gan>

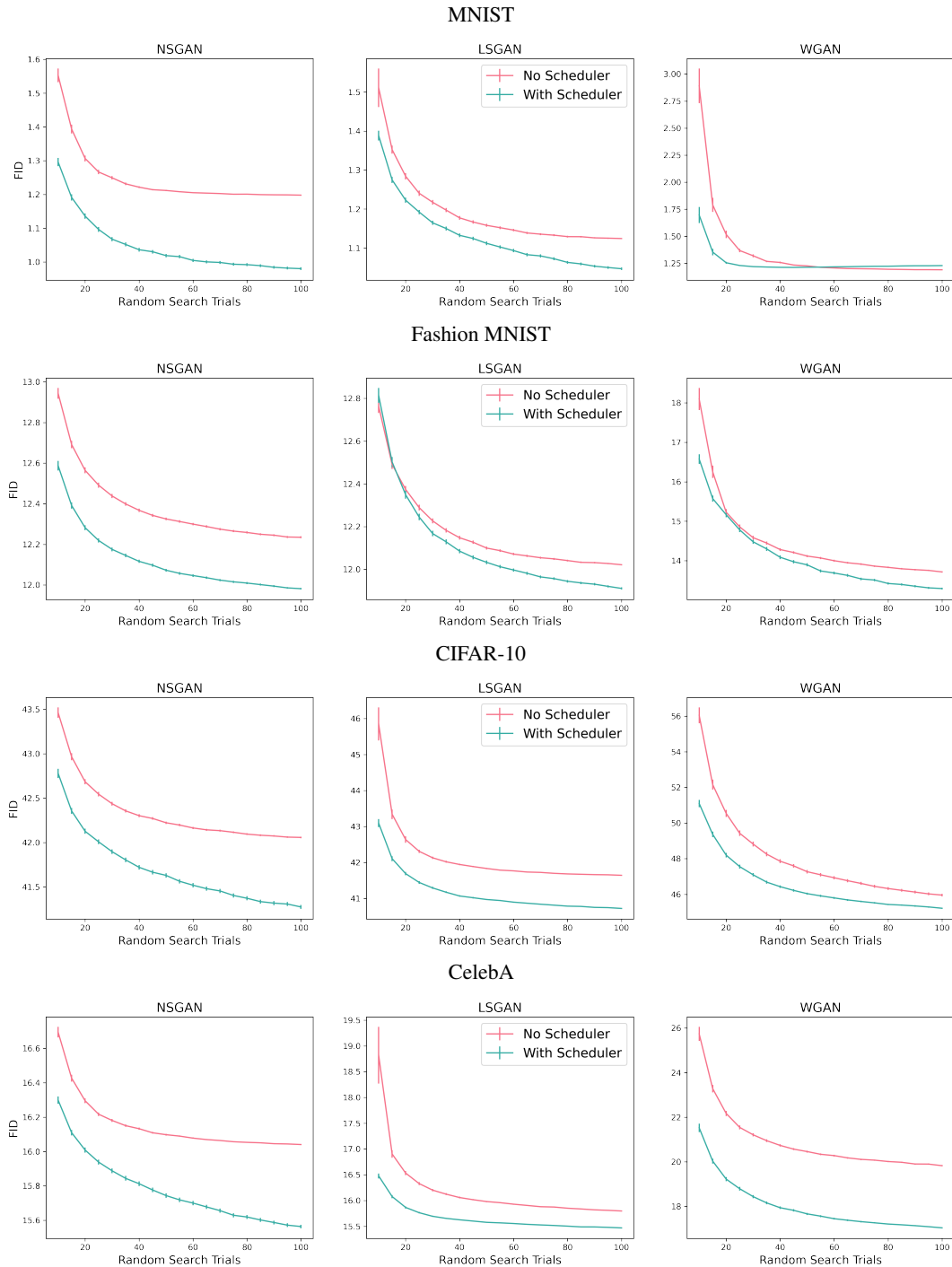


Figure C.3: Decoupled Learning Rates: Plots of the best Frechet Inception Distance (FID) as function of the tuning budget. Following Lucic et al. (2018), for each tuning budget k , we report the mean and 99% confidence intervals of the best FID, estimated using 5,000 bootstrap samples of size k from the original 100 tuning runs. Tuning is performed on a validation set and the FID is reported on a separate test set.

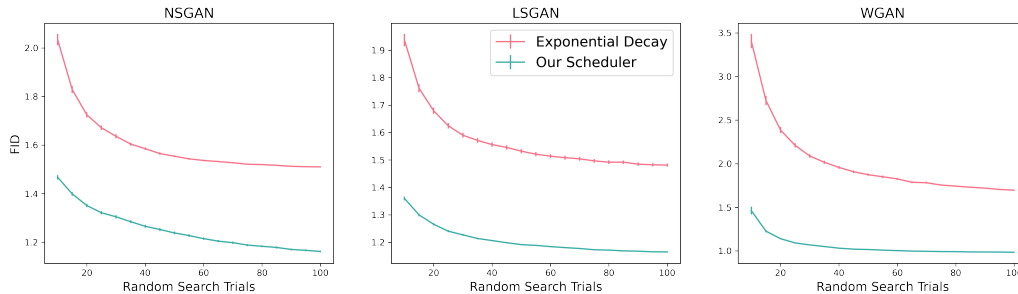


Figure C.4: Exponential Decay vs. Our Scheduler. The exponential decay scheduler decays the base learning rate monotonically (i.e., does not depend on the current state of the network). The exponential decay factor is tuned.

Training: Validation FID is computed every 10 epochs for MNIST, 100 epochs for CIFAR-10 and Fashion MNIST, and 50 epochs for CelebA. Note that we compute FID less often for datasets other than MNIST because the FID computation is expensive (each FID evaluation can take more than 15 minutes on a GPU).

Hyperparameter Ranges: We denote a uniform distribution supported on $[a, b]$ by $U(a, b)$. Moreover, $L(a, b)$ denotes a log-uniform distribution: $x \sim L(a, b) \iff x \sim 10^{U(\log_{10}(a), \log_{10}(b))}$. The hyperparameters are sampled as follows: Learning rate from $L(10^{-5}, 10^{-3})$, β_1 (for Adam) from $U(0, 1)$, and WGAN clipping parameter from $L(10^{-3}, 1)$. Also, note that as discussed in the main paper, we tune the number of epochs by evaluating FID periodically during training.

Architectures: In all architectures, the generator is supplied with a 128-dimensional noise vector, sampled from a standard normal distribution.

MNIST and Fashion MNIST: We use a standard DCGAN architecture (taken from TensorFlow Core examples):

- **Discriminator:** Convolution (64 filters, 5×5 kernel, stride 2, leaky ReLU, batchnorm, dropout 0.3) \rightarrow Convolution (128 filters, 5×5 kernel, stride 2, Leaky ReLU, batchnorm, dropout 0.3) \rightarrow Flatten \rightarrow Dense (1 unit).
- **Generator:** Dense ($7 \times 7 \times 256$), ReLU, batchnorm) \rightarrow Reshape to (7, 7, 256) \rightarrow Up Convolution (128 filters, 5×5 kernel, stride 1, ReLU, batchnorm) \rightarrow Up Convolution (64 filters, 5×5 kernel, stride 2, ReLU, batchnorm) \rightarrow Up Convolution (1 filter, 5×5 kernel, stride 2, Tanh).

CIFAR and CelebA: We use the standard architecture for CIFAR in TF-GAN; with added batchnorm and dropout (to conform with DCGAN).

- **Discriminator:** Convolution (64 filters, 5×5 kernel, stride 2, leaky ReLU, batchnorm, dropout 0.3) \rightarrow Convolution (128 filters, 5×5 kernel, stride 2, Leaky ReLU, batchnorm, dropout 0.3) \rightarrow Convolution (256 filters, 5×5 kernel, stride 2, Leaky ReLU, batchnorm, dropout 0.3) \rightarrow Flatten \rightarrow Dense (1 unit).
- **Generator:** Dense ($4 \times 4 \times 256$), ReLU, batchnorm) \rightarrow Reshape to (4, 4, 256) \rightarrow Up Convolution (128 filters, 5×5 kernel, stride 2, ReLU, batchnorm) \rightarrow Up Convolution (64 filters, 4×4 kernel, stride 2, ReLU, batchnorm) \rightarrow Up Convolution (3 filters, 4×4 kernel, stride 2, Tanh).

D.2 DANN

Dataset and Processing: We use 60,000 images from each of MNIST (labelled) and MNIST-M (unlabelled) during training. We use 5000 samples for each of the validation and test sets in MNIST-M. All pixels in the images are rescaled to $[-1, 1]$.

Hyperparameter Ranges: The hyperparameters are sampled as follows: Learning rate for SGD from $L(10^{-4}, 10^{-2})$, λ uniformly from $\{0.01, 0.1, 1\}$, and V^* from $U(0.5 \log(4), \log(4))$. As discussed in the main text, the number of epochs is tuned during each training run.

Architecture: We consider a simple CNN architecture similar to that in Ganin et al. (2016) (with additional batchnorm and dropout to improve generalization). Below are the architecture details:

Mind the (optimality) Gap: A Gap-Aware Learning Rate Scheduler for Adversarial Nets

- Feature Extractor: Convolution (32 filters, 5×5 kernel, stride 1, ReLU, maxpooling, batchnorm) \rightarrow Convolution (48 filters, 5×5 kernel, stride 1, ReLU, maxpooling, batchnorm) \rightarrow Flatten \rightarrow Dropout (0.3).
- Label Predictor: Dense (100 units, ReLU) \rightarrow Dense (100 units, ReLU) \rightarrow Dense (10 units, Sigmoid).
- Discriminator: Dense (100 units, ReLU) \rightarrow Dense (1 unit, Sigmoid).